Structural Basis of the Disorder in the Tandem Zinc Finger Domain of the RNA-Binding Protein Tristetraprolin

Davide Tavella,[†] Laura M. Deveau,[†] Troy W. Whitfield,[‡,¶] and Francesca Massi[*,†]

Department of Biochemistry and Molecular Pharmacology, University of Massachusetts Medical School, Worcester, MA 01605, Department of Medicine, University of Massachusetts Medical School, Worcester, MA 01605, and Program in Bioinformatics and Integrative Biology, University of Massachusetts Medical School, Worcester, MA 01605

E-mail: francesca.massi@umassmed.edu

Phone: +1 (508) 856-4501. Fax: +1 (508) 856-6464

Supporting Information

[*]To whom correspondence should be addressed

[†]Department of Biochemistry and Molecular Pharmacology, University of Massachusetts Medical School, Worcester, MA 01605

[‡]Department of Medicine, University of Massachusetts Medical School, Worcester, MA 01605

[¶]Program in Bioinformatics and Integrative Biology, University of Massachusetts Medical School, Worcester, MA 01605

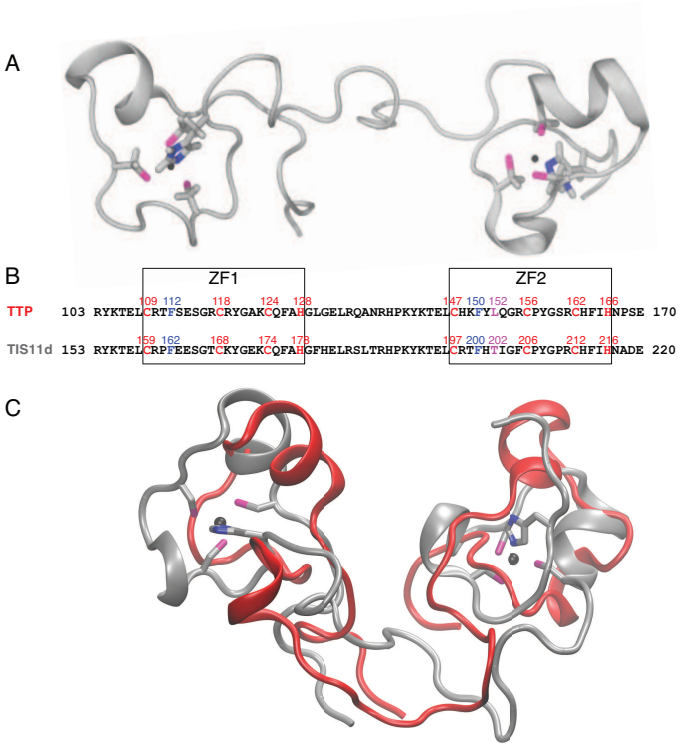

Figure S1: A: NMR solution structure of TIS11d (pdb entry: 1RGO). The side chains of the Zn^{2+}-coordinating residues are shown. Sulfur atoms are depicted in magenta, nitrogen atoms in blue and Zn^{2+} in black. B: Sequence alignment of the tandem zinc finger domains of TIS11d and TTP is shown. Zn^{2+}-coordinating residues are depicted in red, conserved phenylalanines at position Cys^1+3 are depicted in blue. Boxes indicate each zinc finger. C: Equilibrated structures of TIS11d (gray) and TTP (red) from MD trajectories. The side chains of the Zn^{2+}-coordinating residues of TIS11d are shown. Sulfur atoms are depicted in magenta, nitrogen atoms in blue and Zn^{2+} in black. Overall RMSD between the equilibrated structures of the two proteins is in average 8.8 Å, whereas ZF1 and ZF2 show a RMSD < 1 Å and < 1.5 Å, respectively.

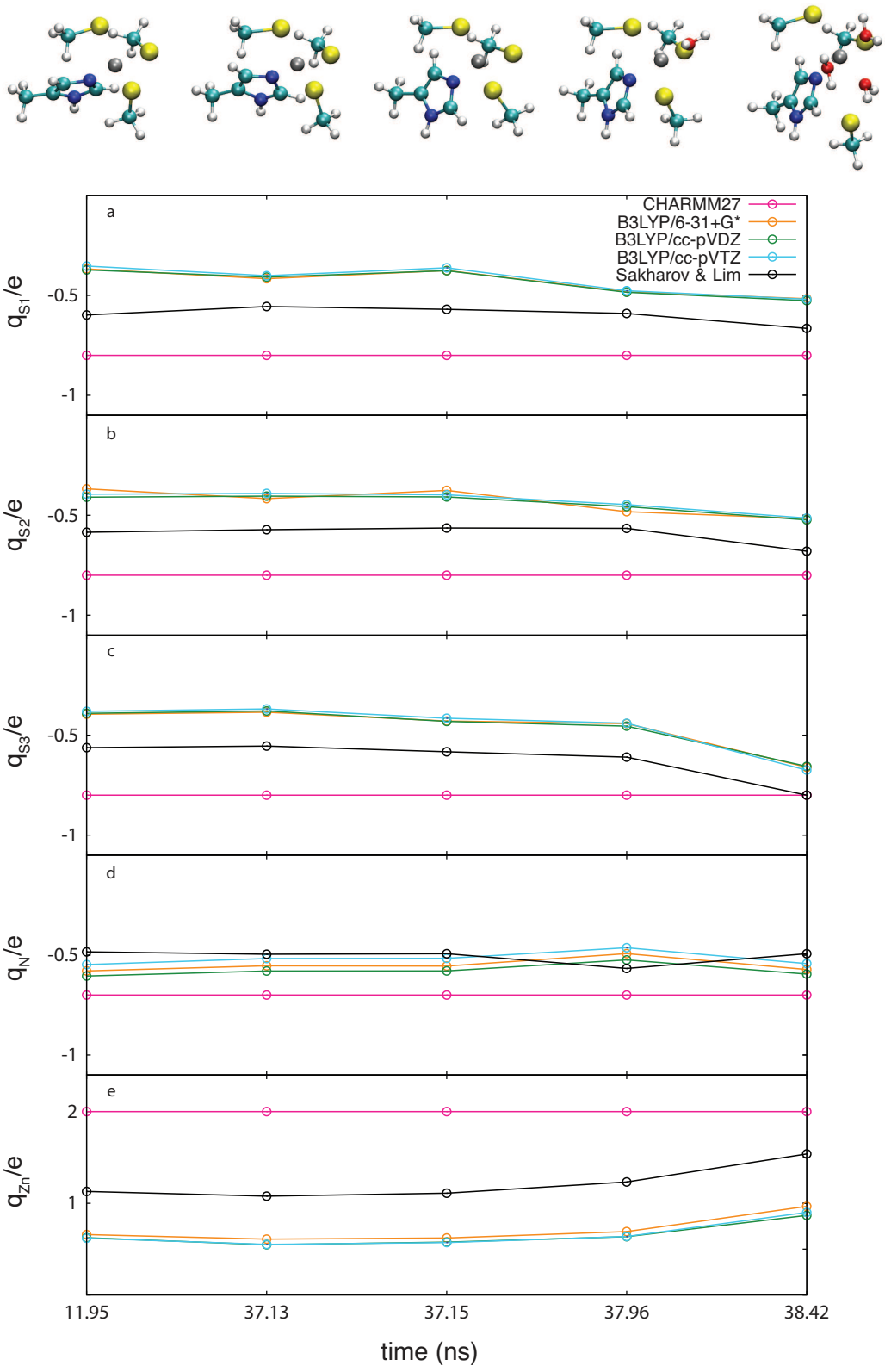
a
b
c
d
e
CHARMM27
B3LYP/6-31+G*
B3LYP/cc-pVDZ
B3LYP/cc-pVTZ
Sakharov & Lim
q_{S1}/e
q_{S2}/e
q_{S3}/e
q_N/e
q_{Zn}/e
-0.5
-1
2
1
11.95
37.13
37.15
37.96
38.42
time (ns)

Figure S2

Figure S2: Classical polarizable charge-transfer model approximates environmental dependence of electrostatic charges in the zinc fingers of TTP/TIS11d throughout molecular dynamics simulations. In order to evaluate the accuracy of the zinc finger model of Sakharov and Lim[1] in classical molecular dynamics simulations of TTP and TIS11d, five configurations of ZF2 in TTP were extracted from a single trajectory to represent different states of zinc coordination (these configurations are visualized at the top of the figure above), ranging from fully coordinated by the CCCH residues (leftmost three configurations) to partially coordinated (rightmost two configurations). As a reference, the charges were computed using density functional theory with the B3LYP approximate exchange-correlation functional[2–4] using Gaussian09[5], after truncating the protein backbone atoms from the cysteine and histidine residues to form methanethiolate anions and a 4-methylimidazole molecule, respectively. The charges from the CHARMM27[6] force field are compared with those from the polarizable charge-transfer model of Sakharov and Lim[1] along with the natural bond orbital (NBO) charges[7–10] corresponding to a series of different basis sets. The 6-31+G* basis set was used in the parameterization of the CHARMM27[6] force field, along with that of the Sakharov and Lim[1] model. Shown for comparison are the cc-pVDZ and cc-pVTZ basis sets. Agreement among the different basis sets suggests that these choices are adequate, as basis set expansion yields very small changes in the charges. Panels (a-c) report the charges on the sulfur atom of the methanethiolate anion, panel (d) reports the charge on the zinc-coordinating nitrogen atom of the 4-methylimidazole molecule, while (e) reports the charge on the zinc cation. In each configuration, the polarizable charge-transfer model represents an improved approximation to the fixed-charge model.

Table S1: Values of RMSD for the equilibrated structures of the protein and ZF1 and ZF2, calculated for six trajectories 100 ns long of TIS11d and three trajectories 100 ns long for TTP. Values are shown as mean ± STD.

	RMSD(protein) (Å)	RMSD(ZF1) (Å)	RMSD(ZF2) (Å)
TIS11d r1	7.388 ± 2.320	0.808 ± 0.123	0.587 ± 0.117
TIS11d r2	7.136 ± 2.226	0.693 ± 0.151	0.675 ± 0.173
TIS11d r3	3.293 ± 0.565	0.520 ± 0.112	0.512 ± 0.108
TIS11d r4	3.767 ± 1.697	0.526 ± 0.103	0.627 ± 0.236
TIS11d r5	5.353 ± 2.505	0.568 ± 0.147	0.601 ± 0.128
TIS11d r6	1.638 ± 0.721	0.568 ± 0.118	0.499 ± 0.136
TTP r1	5.216 ± 1.214	0.520 ± 0.126	1.410 ± 0.354
TTP r2	7.540 ± 1.770	0.605 ± 0.133	0.663 ± 0.147
TTP r3	4.314 ± 2.678	0.595 ± 0.156	0.596 ± 0.159

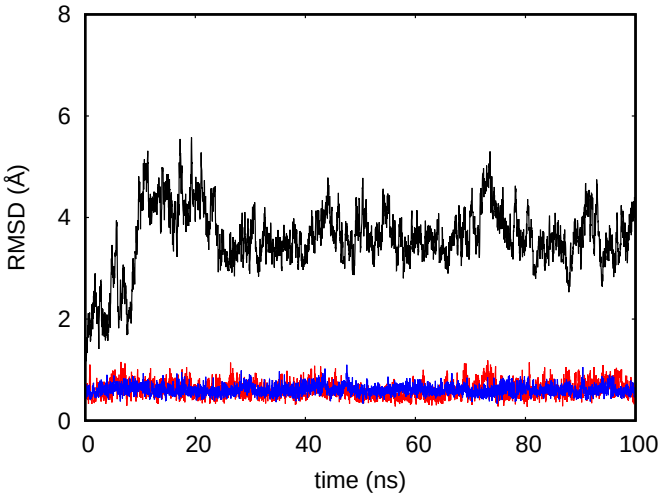

Figure S3: RMSD as a function of time for a representative 100 ns long trajectory of TIS11d. RMSD for the overall protein is depicted in black, for ZF1 in red and for ZF2 in blue.

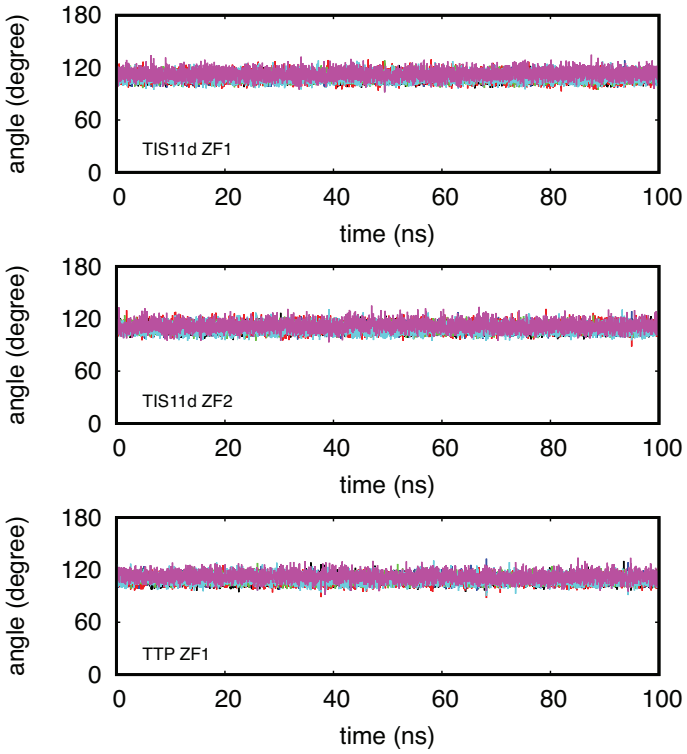

Figure S4: The geometry of the zinc coordination in both zinc fingers of TIS11d and in ZF1 of TTP is monitored. The angles between the zinc ion and the zinc coordinating atoms are shown for a representative 100 ns long trajectory of TIS11d and for the 100 ns long trajectory of TTP where zinc coordination is lost: $\measuredangle \mathrm{S}^{Cys^1}\text{-}\mathrm{Zn}^{2+}\text{-}\mathrm{S}^{Cys^2}$ in black, $\measuredangle \mathrm{S}^{Cys^1}\text{-}\mathrm{Zn}^{2+}\text{-}\mathrm{S}^{Cys^3}$ in blue, $\measuredangle \mathrm{S}^{Cys^1}\text{-}\mathrm{Zn}^{2+}\text{-}\mathrm{N}_{\varepsilon}^{His^4}$ in red, $\measuredangle \mathrm{S}^{Cys^2}\text{-}\mathrm{Zn}^{2+}\text{-}\mathrm{S}^{Cys^3}$ in green, $\measuredangle \mathrm{S}^{Cys^2}\text{-}\mathrm{Zn}^{2+}\text{-}\mathrm{N}_{\varepsilon}^{His^4}$ in cyan and $\measuredangle \mathrm{S}^{Cys^3}\text{-}\mathrm{Zn}^{2+}\text{-}\mathrm{N}_{\varepsilon}^{His^4}$ in magenta.

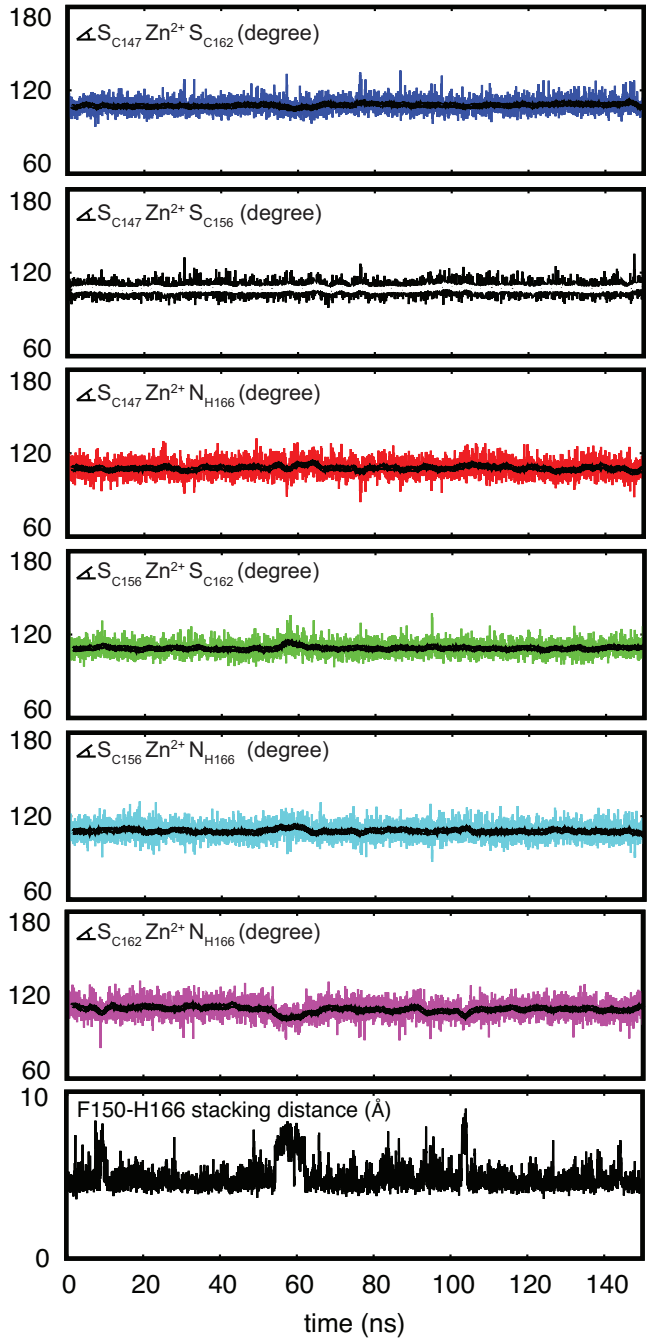

Figure S5: The geometry of the zinc coordination in the C-terminal zinc finger of TTP is monitored. The angles between the zinc ion and the zinc coordinating atoms are shown for the first trajectory of TTP, 150 ns long: $\measuredangle \mathrm{S}^{C147}\text{-}\mathrm{Zn}^{2+}\text{-}\mathrm{S}^{C156}$ in black, $\measuredangle \mathrm{S}^{C147}\text{-}\mathrm{Zn}^{2+}\text{-}\mathrm{S}^{C162}$ in blue, $\measuredangle \mathrm{S}^{C147}\text{-}\mathrm{Zn}^{2+}\text{-}\mathrm{N}_{\varepsilon}^{H166}$ in red, $\measuredangle \mathrm{S}^{C156}\text{-}\mathrm{Zn}^{2+}\text{-}\mathrm{S}^{C162}$ in green, $\measuredangle \mathrm{S}^{C156}\text{-}\mathrm{Zn}^{2+}\text{-}\mathrm{N}_{\varepsilon}^{H166}$ in cyan and $\measuredangle \mathrm{S}^{C162}\text{-}\mathrm{Zn}^{2+}\text{-}\mathrm{N}_{\varepsilon}^{H166}$ in magenta. Stacking distance between F150 and H166 is shown as a function of time. The distance between the aromatic rings was calculated as the distance between the centers of mass for the heavy atoms of the two side chains. The running average of the angles, calculated for a window of 100 datapoints, is shown as a black line (white for $\measuredangle \mathrm{S}^{C147}\text{-}\mathrm{Zn}^{2+}\text{-}\mathrm{S}^{C156}$) within each plot.

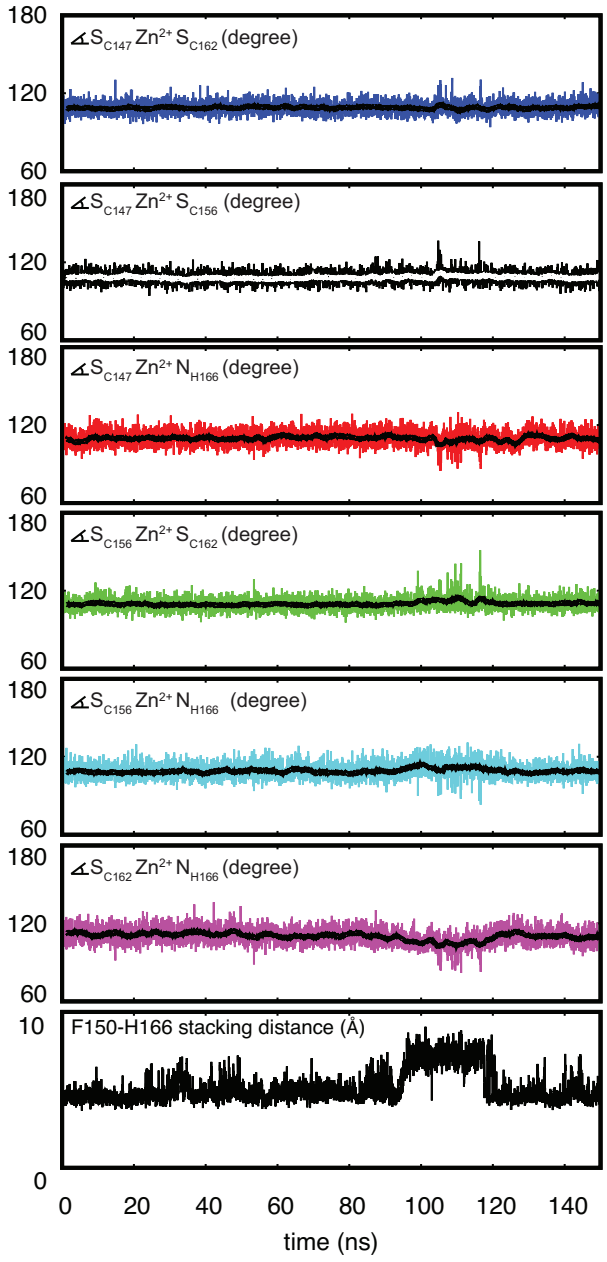

Figure S6: The geometry of the zinc coordination in the C-terminal zinc finger of TTP is monitored. The angles between the zinc ion and the zinc coordinating atoms are shown for the second trajectory of TTP, 150 ns long: $\measuredangle \mathrm{S}^{C147}\text{-}\mathrm{Zn}^{2+}\text{-}\mathrm{S}^{C156}$ in black, $\measuredangle \mathrm{S}^{C147}\text{-}\mathrm{Zn}^{2+}\text{-}\mathrm{S}^{C162}$ in blue, $\measuredangle \mathrm{S}^{C147}\text{-}\mathrm{Zn}^{2+}\text{-}\mathrm{N}_{\varepsilon}^{H166}$ in red, $\measuredangle \mathrm{S}^{C156}\text{-}\mathrm{Zn}^{2+}\text{-}\mathrm{S}^{C162}$ in green, $\measuredangle \mathrm{S}^{C156}\text{-}\mathrm{Zn}^{2+}\text{-}\mathrm{N}_{\varepsilon}^{H166}$ in cyan and $\measuredangle \mathrm{S}^{C162}\text{-}\mathrm{Zn}^{2+}\text{-}\mathrm{N}_{\varepsilon}^{H166}$ in magenta. Stacking distance between F150 and H166 is shown as a function of time. The distance between the aromatic rings was calculated as the distance between the centers of mass for the heavy atoms of the two side chains. The running average of the angles, calculated for a window of 100 datapoints, is shown as a black line (white for $\measuredangle \mathrm{S}^{C147}\text{-}\mathrm{Zn}^{2+}\text{-}\mathrm{S}^{C156}$) within each plot.

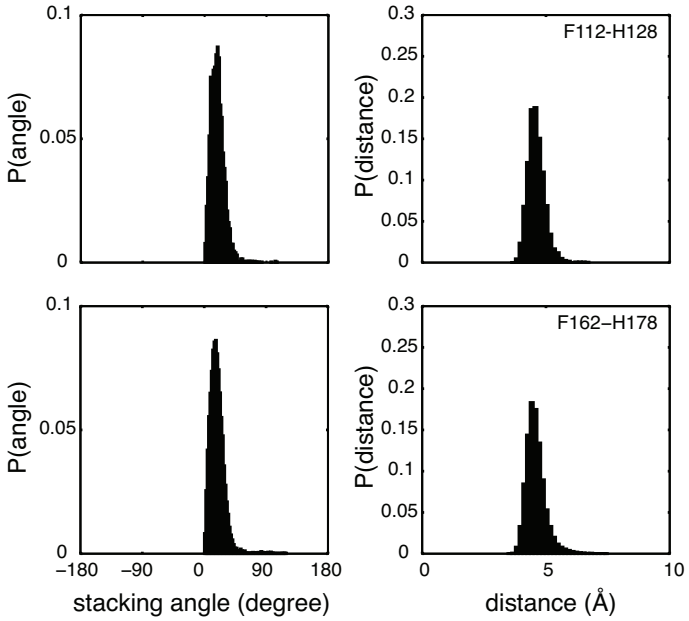

Figure S7: Aromatic side chain stacking of phenylalanine and histidine in ZF1 of TTP (top) and TIS11d (bottom). Probability distribution of the stacking angle (left), calculated as the angle between the normals of the two aromatic rings (the planes for the side chains are defined by atoms C_{δ_2}, C_{ε_1} and N_{ε_2} for histidine and C_ζ, C_{ε_2},C_{δ_2} for phenylalanine). Probability distribution of the distance between the aromatic rings (right), calculated as the distance between the centers of mass of the heavy atoms of the two side chains. Data refer to the 100 ns long unfolding MD trajectory for TTP and to six 100 ns long MD trajectory for TIS11d.

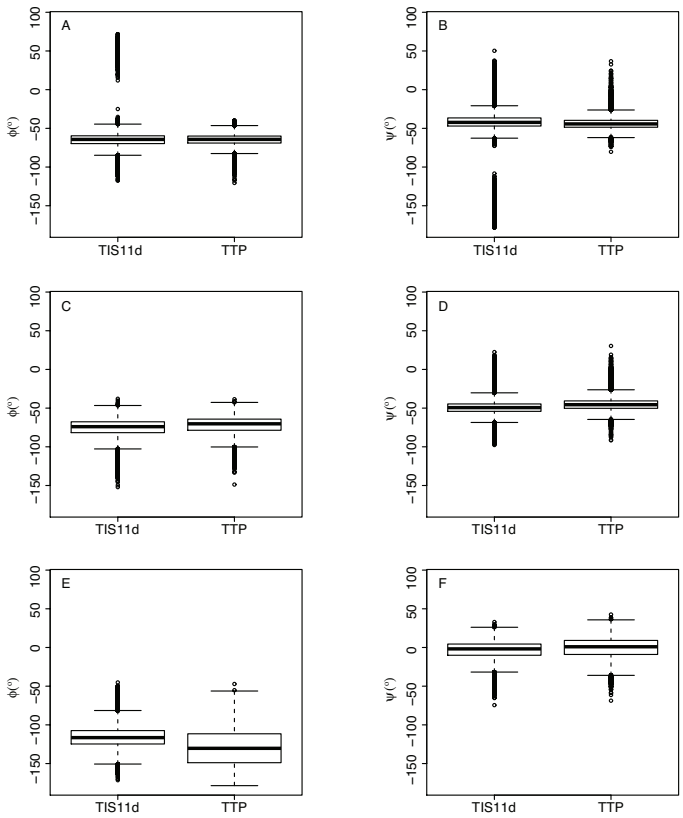

Figure S8: Box-and-whisker plots of the distribution of ϕ and ψ angles for residues 201 (A,B), 202 (C,D), 203 (E,F) of TIS11d and 151 (A,B), 152 (C,D), 153 (E,F) of TTP. Data refer to the 100 ns long unfolding MD trajectory for TTP and to six 100 ns MD trajectories for TIS11d. The outlier points in panels A and B for TIS11d, centered at $\phi = 50°$ and $\psi = -150°$, correspond to a single event observed in one trajectory where a hydrogen bond within the α-helix is transiently lost.

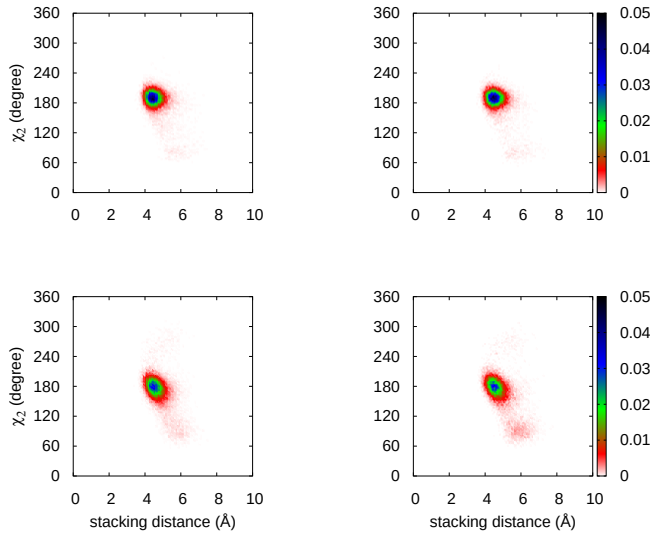

Figure S9: The T202L mutant form of TIS11d samples the Zn^{2+} binding-incompatible state with higher probability than wild type. Probability density distribution of the dihedral angles χ_2 of H178 and the stacking distance of F162 and H178 in ZF1 of TIS11d (top left), χ_2 of H216 and the stacking distance of F200 and H216 in ZF2 of TIS11d (bottom left), χ_2 of H128 and the stacking distance of F112 and H128 in ZF1 of TIS11d T202L (top right), χ_2 of H166 and the stacking distance of F150 and H166 in ZF2 of TIS11d T202L (bottom right). Data are taken from six 100 ns MD trajectories of TIS11d wild type and from six 100 ns MD trajectories of TIS11d T202L. The color bars show the values of the probability density calculated for χ_2 and stacking distance as the number of counts normalized by the total number of observations and by the area of each bin.

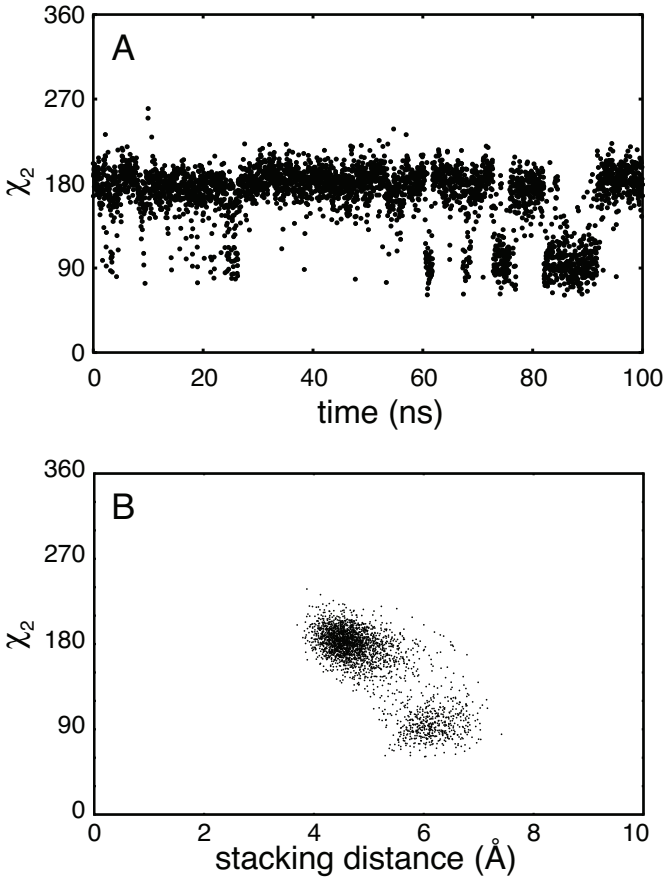

Figure S10: A: The χ_2 dihedral angle of the side chain of H216 is shown as a function of time for a representative 100 ns long trajectory of the TIS11d T202L mutant. B: Scatter plot of the stacking distance between the aromatic ring of F200 and H216 and the χ_2 dihedral angle of H216 for the TIS11d T202L mutant. The distance between the aromatic rings was calculated as the distance between the centers of mass for the heavy atoms of the two side chains. Data were extracted from a representative 100 ns long trajectory of the TIS11d T202L mutant.

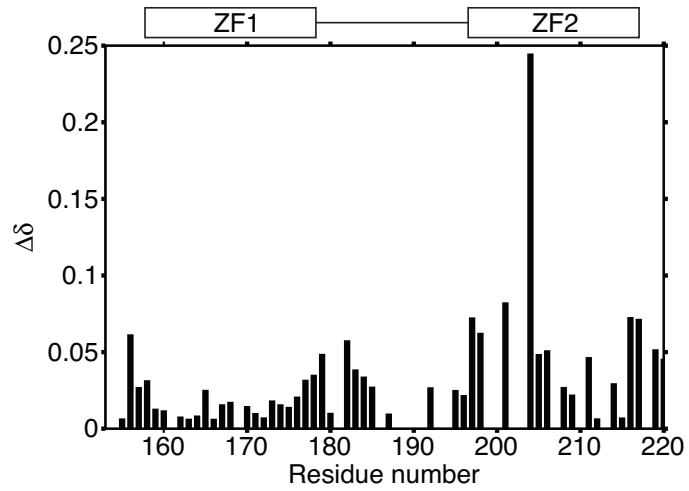

Figure S11: Chemical shift difference between the ^{15}N-^{1}H HSQC spectra of TIS11d T202L and TIS11d wild type. $\Delta\delta$ was calculated as $\sqrt{\left(\Delta\delta_{^{15}N} \cdot \frac{\gamma_{^{15}N}}{\gamma_{^{1}H}}\right)^2 + \left(\Delta\delta_{^{1}H}\right)^2}$.

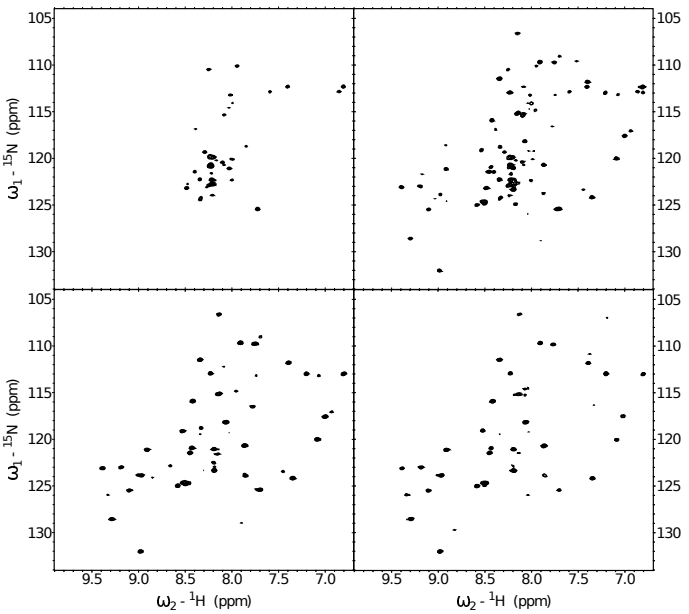

Figure S12: Zn^{2+} titration of TIS11d T202L followed by NMR spectroscopy. The ^{15}N-^{1}H HSQC spectra correspond to the protein in absence of zinc (top left), protein with 0.5 equivalents of zinc in solution (top right), protein with 1 equivalent of zinc in solution (bottom left) and protein with 3-fold excess of zinc (bottom right). Cross-peaks from ZF2 have low intensities, close to the noise.

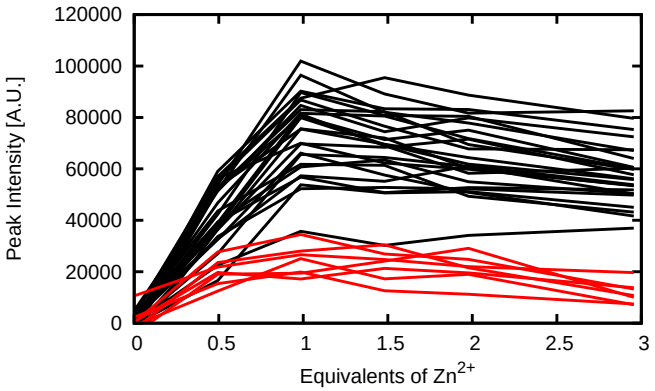

Figure S13: Zn^{2+} titration of TIS11d T202L followed by NMR spectroscopy. Cross-peak intensities from the ^{15}N-^{1}H HSQC spectra are shown as a function of zinc concentration. Cross-peak intensities of residues 155-186 are depicted in black, 187-220 in red. The overall decrease in intensity observed at high zinc concentration is due to a small change in pH upon $ZnSO_4$ addiction.

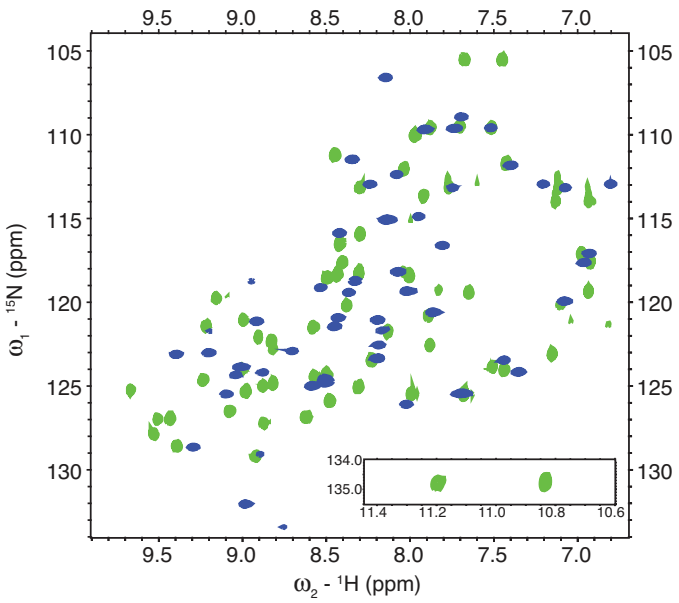

Figure S14: ^{15}N-^{1}H HSQC spectra of TIS11d T202L free (blue) and bound (green) to 5′-UUUAUUUAUUUU-3′ RNA.

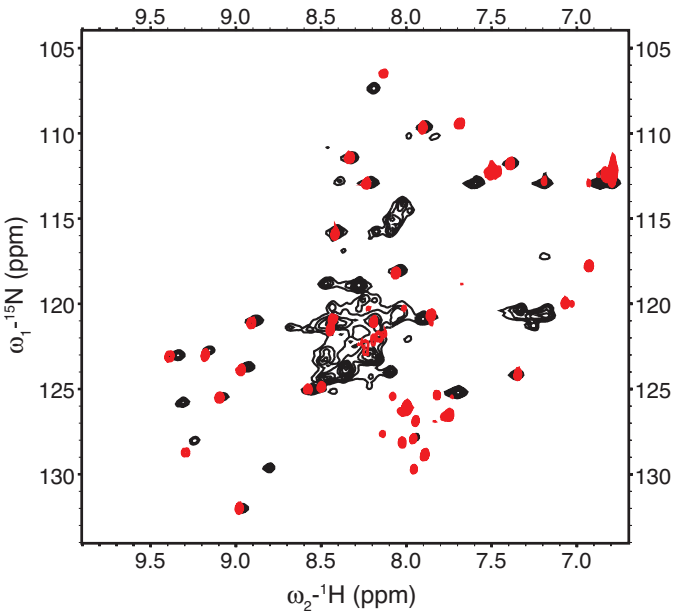

Figure S15: Comparison of ^{15}N-^{1}H HSQC spectra of TIS11d F200A (red) and TIS11d C212S (black).

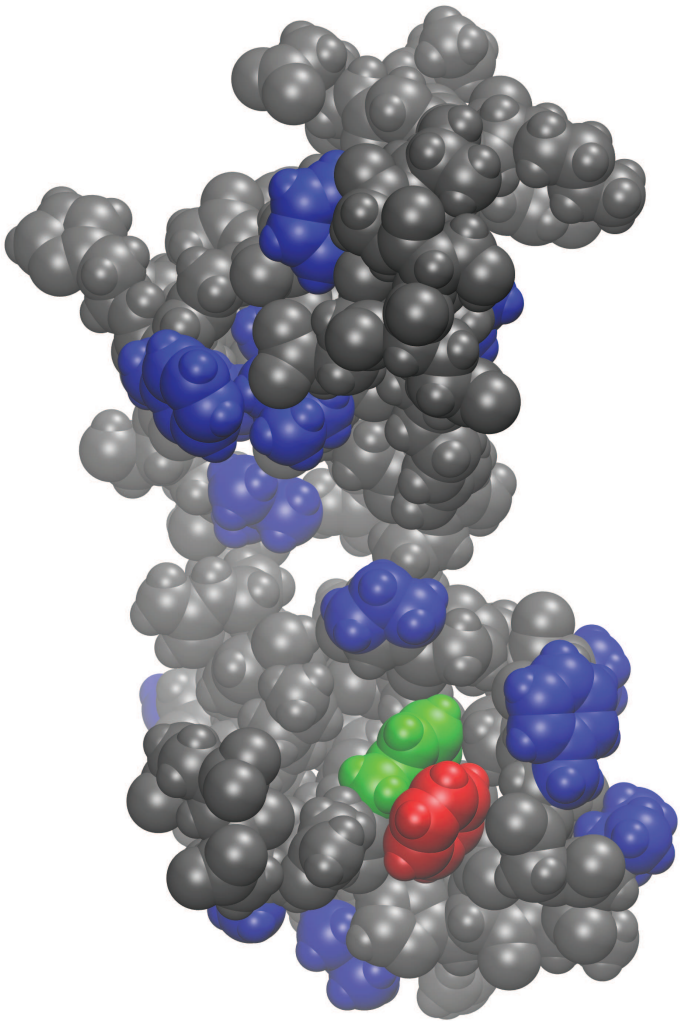

Figure S16: All atoms representation of the NMR solution structure of TIS11d (pdb entry: 1RGO). Side chains of hydrophobic residues are depicted in blue, side chain of F200 in red and side chain of H216 in green.

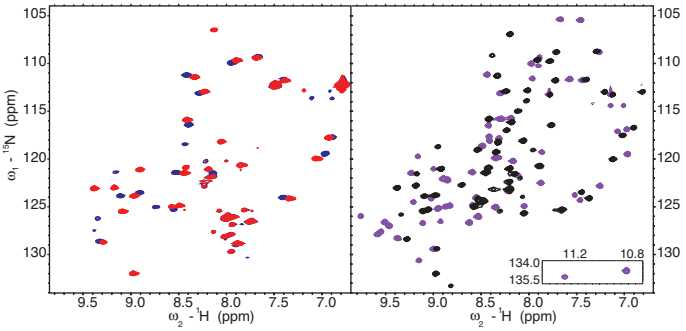

Figure S17: ^{15}N-^{1}H HSQC spectra of TIS11d F200A free (red) and bound (blue) to 5′-UUUAUUUAUUUU-3′ RNA compared to the spectra of TIS11d wild type free (black) and bound (purple) to 5′-UUUAUUUAUUUU-3′ RNA.

References

(1) Sakharov, D. V.; Lim, C. *J. Am. Chem. Soc.* **2004**, *127*, 4921–4929.

(2) Becke, A. D. *Phys. Rev. A* **1988**, *38*, 3098–3100.

(3) Lee, C.; Yang, W.; Parr, R. G. *Phys. Rev. B* **1988**, *37*, 785–789.

(4) Becke, A. D. *J. Chem. Phys.* **1993**, *98*, 5648–5652.

(5) Frisch, M. J.; Trucks, G. W.; Schlegel, H. B.; Scuseria, G. E.; Robb, M. A.; Cheeseman, J. R.; Scalmani, G.; Barone, V.; Mennucci, B.; Petersson, G. A.; Nakatsuji, H.; Caricato, M.; Li, X.; Hratchian, H. P.; Izmaylov, A. F.; Bloino, J.; Zheng, G.; Sonnenberg, J. L.; Hada, M.; Ehara, M.; Toyota, K.; Fukuda, R.; Hasegawa, J.; Ishida, M.; Nakajima, T.; Honda, Y.; Kitao, O.; Nakai, H.; Vreven, T.; Montgomery, J. A., Jr.; Peralta, J. E.; Ogliaro, F.; Bearpark, M.; Heyd, J. J.; Brothers, E.; Kudin, K. N.; Staroverov, V. N.; Kobayashi, R.; Normand, J.; Raghavachari, K.; Rendell, A.; Burant, J. C.; Iyengar, S. S.; Tomasi, J.; Cossi, M.; Rega, N.; Millam, J. M.; Klene, M.; Knox, J. E.; Cross, J. B.; Bakken, V.; Adamo, C.; Jaramillo, J.; Gomperts, R.; Stratmann, R. E.; Yazyev, O.; Austin, A. J.; Cammi, R.; Pomelli, C.; Ochterski, J. W.;

Martin, R. L.; Morokuma, K.; Zakrzewski, V. G.; Voth, G. A.; Salvador, P.; Dannenberg, J. J.; Dapprich, S.; Daniels, A. D.; Farkas, O.; Foresman, J. B.; Ortiz, J. V.; Cioslowski, J.; Fox, D. J. Gaussian 09 Revision E.01. Gaussian Inc. Wallingford CT 2009.

(6) MacKerell, A. D.; Bashford, D.; Bellott, M.; Dunbrack, R. L.; Evanseck, J. D.; Field, M. J.; Fischer, S.; Gao, J.; Guo, H.; Ha, S.; Joseph-McCarthy, D.; Kuchnir, L.; Kuczera, K.; Lau, F. T. K.; Mattos, C.; Michnick, S.; Ngo, T.; Nguyen, D. T.; Prodhom, B.; Reiher, W. E.; Roux, B.; Schlenkrich, M.; Smith, J. C.; Stote, R.; Straub, J.; Watanabe, M.; Wiorkiewicz-Kuczera, J.; Yin, D.; Karplus, M. *J Phys Chem B J Phys Chem B* **1998**, *102*, 3586–3616.

(7) Foster, J. P.; Weinhold, F. *J. Am. Chem. Soc.* **1980**, *102*, 7211–7218.

(8) Reed, A. E.; Weinhold, F. *J. Chem. Phys.* **1983**, *78*, 4066–4073.

(9) Reed, A. E.; Weinstock, R. B.; Weinhold, F. *J. Chem. Phys.* **1985**, *83*, 735–746.

(10) Reed, A. E.; Weinhold, F. *J. Chem. Phys.* **1985**, *83*, 1736–1740.